The Reactivity of C(^{1}D) with Oxygen Bearing Molecules NO and O_2 at Low Temperature

Dianailys Nuñez-Reyes[a,b] *and Kevin M. Hickson**,[a,b]

[a] Université de Bordeaux, Institut des Sciences Moléculaires, F-33400 Talence, France

[b] CNRS, Institut des Sciences Moléculaires, F-33400 Talence, France

AUTHOR INFORMATION

Corresponding Author

kevin.hickson@u-bordeaux.fr

+33 5 40 00 63 42

Keywords

Gas-phase reactions; low temperature; rate constants; Laval nozzle reactor.

Highlights

Low temperature rate constants were measured using a chemical tracer method.

The reaction of $C(^1D)$ with NO has a negative temperature dependence.

The reaction of $C(^1D)$ with O_2 does not display a marked temperature dependence.

Secondary reactions have a minor influence on the rate constant determination.

Abstract

The gas-phase reactions, $C(^1D)$ + NO and $C(^1D)$ + O_2 have been studied over the 50-296 K range using a Laval nozzle reactor. $C(^1D)$ atoms were produced by CBr_4 photolysis. A tracer technique was employed to follow the kinetics by adding H_2 or CH_4 to the flow. H-atoms produced by the $C(^1D)$ + H_2/CH_4 reactions were detected by laser-induced fluorescence. Rate constants for the $C(^1D)$ + O_2 reaction show little variation with temperature, whereas rate constants for the $C(^1D)$ + NO reaction increase rapidly below 100 K. Numerical simulations were performed to evaluate the influence of secondary reactions.

1 Introduction

The gas-phase reactions of atomic carbon are important processes in a variety of different environments and over a wide temperature range. In this respect, numerous experimental studies of the kinetics [1-8] and dynamics [9-13] of ground state atomic carbon reactions have been performed, providing detailed information regarding the mechanistic aspects of both radical-molecule and radical-radical reactions involving $C(^3P)$. The reactivity of excited state $C(^1D)$ atoms is less well understood, except for certain prototypical reactions such as $C(^1D) + H_2 \rightarrow CH + H$; a process which is simple enough to allow rigorous comparison between the most elaborate theoretical calculations and experiment [14-21]. In addition, a few detailed dynamics investigations of the reactivity of $C(^1D)$ atoms with hydrocarbons have been performed [22-24]. To address this issue, we have initiated a series of measurements to investigate both reactive and non-reactive processes involving $C(^1D)$ atoms, with a particular focus on their interactions with closed shell molecules [7,18,19,25,26]. Even less is known about the reactivity of $C(^1D)$ towards open shell species such as NO or towards biradicals such as O_2, although the kinetics of the equivalent ground state carbon atom reactions have already been studied [3].

The ground state reagents $C(^3P)$ and $NO(X^2\Pi)$ correlate adiabatically with $CN(X^2\Sigma^+)/CN(A^2\Pi) + O(^3P)$, $CO(X^1\Sigma^+) + N(^2D)$ and $CO(X^1\Sigma^+) + N(^4S)$ as exothermically allowed products. Indeed, several of these channels have been identified experimentally [27] and the reaction is characterized by a fast rate constant that increases to low temperature [3,27-31]. For the $C(^1D) + NO(X^2\Pi)$ reaction, although an additional channel yielding $CN(X^2\Sigma^+) + O(^1D)$ products is expected to be open, ground state $CO(X^1\Sigma^+) + N(^4S)$ product formation is spin-forbidden despite the highly exothermic nature of this process (-567 kJ mol^{-1}); a fact which might influence the overall reactivity. Interestingly, earlier kinetic studies of the $C(^1D)$ + NO reaction

at room temperature [32] indicate that it could be significantly slower than the reaction between ground state reagents.

In the case of the $C(^3P) + O_2(X^3\Sigma_g^-)$ reaction, the spin-allowed exothermic products are $CO(X^1\Sigma^+) + O(^3P)$ and $CO(X^1\Sigma^+) + O(^1D)$, although experimental evidence suggests that the favored exit channel is not the one leading to ground state products [31]. The equivalent reaction with $C(^1D)$ could lead to the formation of $CO(X^1\Sigma^+/a^3\Pi) + O(^3P)$ as possible products because the $CO(X^1\Sigma^+) + O(^1D)$ channel is spin-forbidden. Previous studies of the $C(^3P)/C(^1D) + O_2$ reactions also indicate that the $C(^1D)$ reaction occurs less efficiently than the $C(^3P)$ one [32] at room temperature, although no information exists regarding the relative reactivity of these processes over a range of temperatures.

Here we report the results of an experimental investigation of the $C(^1D) + NO$ and $C(^1D) + O_2$ reactions in the gas-phase. Rate constants for these processes were measured over the 50 - 296 K temperature range using a Laval nozzle reactor coupled with pulsed laser photolysis to produce $C(^1D)$ atoms, employing a chemical tracer method to follow the reaction kinetics. Section 2 presents the method used to perform this study. Section 3 describes the outcome of these experiments and discusses the validity of the results through modeling studies of the processes occurring within the reactor. Our conclusions are presented in Section 4.

2 Experimental Section

The experiments reported here were performed using a supersonic flow reactor operating in continuous mode [33,34], with the low temperature flows being generated by axisymmetric Laval nozzles. Although a wide range of nozzles is available in our laboratory employing a variety of carrier gases (Ar, N_2 or N_2/SF_6 mixtures) to access temperatures in the range 50-240 K, only argon based nozzles were used during this study. The fast removal of excited state

carbon atoms by molecular colliders excluded the use of any of the N_2 based nozzles [25]. The measured and calculated flow properties of the Laval nozzles used here are listed in Table 1.

Table 1 Characteristics of the supersonic flows

Mach number	2.0 ± 0.03[a]	3.0 ± 0.1	3.9 ± 0.1
Carrier gas	Ar	Ar	Ar
Density ($\times 10^{16}$ cm^{-3})	12.6 ± 0.3	14.7 ± 0.6	25.9 ± 0.9
Impact pressure (Torr)	10.5 ± 0.2	15.3 ± 0.5	29.6 ± 1.0
Stagnation pressure (Torr)	13.9	34.9	113
Temperature (K)	127 ± 2	75 ± 2	50 ± 1
Mean flow velocity (ms^{-1})	419 ± 3	479 ± 3	505 ± 1
Chamber pressure (Torr)	1.5	1.2	1.4

[a] The errors on the Match number, density, temperature and mean flow velocity (1σ) are calculated from separate measurements of the impact pressure using a Pitot tube as a function of distance from the Laval nozzle and the stagnation pressure within the reservoir.

Measurements were also performed at room temperature, by removing the Laval nozzle and by reducing the flow velocity to eliminate pressure and temperature gradients within the reactor. The pulsed laser photolysis method was used to generate C(^{1}D) in these experiments, through the 266 nm multiphoton dissociation of CBr_4 as the atom source using a frequency quadrupled Nd:YAG laser, with the laser beam aligned along the supersonic flow axis. This process produces mostly ground state C(^{3}P) atoms with relative yields of C(^{1}D) atoms in the 10-15 % range as already observed in a previous study [7]. A small argon flow directed into a vessel containing solid CBr_4 maintained at a known pressure and temperature allowed CBr_4 vapour to be carried into the Laval nozzle reservoir. CBr_4 concentrations did not exceed 1.7×10^{13} molecule cm^{-3} within the supersonic flow. C(^{1}D) atoms could not be observed directly in the present experiments because no strong transitions originating from the ^{1}D state were accessible using our current detection method. Instead, small quantities of H_2 or CH_4 were added to the

supersonic flow, allowing us to follow the H-atom products of the $C(^1D) + H_2 \rightarrow CH + H$ reaction or through one of the major channels of the $C(^1D) + CH_4$ reaction (leading to $H_2CC/C_2H_2 + H + H$ as products) by vacuum ultraviolet laser induced fluorescence (VUV LIF) using the $1s\ ^2S \rightarrow 2p\ ^2P^0$ Lyman-α transition at 121.567 nm. Both processes produce atomic hydrogen with yields close to unity [18,26], while $C(^3P)$ atoms themselves are unreactive with both H_2 and CH_4 at room temperature and below. A more detailed explanation of the methodology used to extract rate constants for the $C(^1D) + NO/O_2$ reactions is provided in the results and discussion section. Tunable light around 121.6 nm was produced through third harmonic generation by focusing a UV laser beam at 364.7 nm produced by a Nd:YAG pumped dye laser into a cell containing 210 Torr of krypton and 540 Torr of argon for phase matching purposes [7]. The resulting VUV radiation was collimated by a MgF_2 lens that also served as the cell window. The cell was attached to the reactor at the level of the detection axis via a 75 cm sidearm containing baffles that effectively prevented most of the divergent UV light from entering the reactor. Moreover, the sidearm was constantly flushed with N_2 or Ar during the experiments to prevent the attenuation of VUV radiation by residual reactive gases in this region. The VUV LIF emission itself was collected by a solar blind photomultiplier tube coupled with a boxcar integrator for signal acquisition and processing.

Gases were flowed directly from cylinders through calibrated digital mass flow controllers into the reactor. The stated purities are (Linde Ar 99.999%, O_2 99.999%, Kr 99.99% CH_4 99.9995%, Air Liquide N_2 99.999%, H_2 99.9999% and NO 99.9%).

3 Results and discussion

For any series of measurements, the H_2 or CH_4 concentrations were set to a fixed value (in large excess with respect to $C(^1D)$ atoms) so that in the absence of competing secondary reactions, the temporal evolution of the H-atom VUV LIF signal could be described using the formula

$$I_H = A\{exp(-k'_L t) - exp(-k'_F t)\} \quad (1)$$

where A is the H-atom signal amplitude and k'_F and k'_L are the pseudo-first-order rate constants for H-atom formation and loss respectively.

k'_L represents the first-order loss rate of atomic hydrogen and has contributions from diffusion $k_{diff,H}$ as well as secondary reactions $k_{H+X}[X]$.

k'_F governs the rise time of the H-atom signal and comprises the following terms:

$$\sum k_{C(^1D)+Y}[Y] + k_{C(^1D)+Z}[Z] + k_{C(^1D)+CBr_4}[CBr_4] + k_{C(^1D)+Ar}[Ar] + k_{diff,C(^1D)}$$

$k_{C(^1D)+Y}[Y]$ is the pseudo-first-order rate for the reaction of C(^{1}D) with Y where Y is H_2 or CH_4, $k_{C(^1D)+CBr_4}[CBr_4]$ is the pseudo-first-order rate for the reaction of C(^{1}D) with CBr_4, $k_{C(^1D)+Ar}[Ar]$ is the pseudo-first-order rate for the removal of C(^{1}D) by Ar and $k_{diff,C(^1D)}$ is the first-order diffusional loss rate of C(^{1}D). All these terms are constant for any single series of measurements. $k_{C(^1D)+Z}[Z]$ is the pseudo-first-order rate for the reaction of C(^{1}D) with Z where Z is NO or O_2. NO or O_2 **are** systematically varied so that k'_F varies as a function of $[Z]$ for any single series of measurements. Both NO and O_2 were used in large excess with respect to C(^{1}D) atoms so that the pseudo-first-order approximation was valid.

The measured H-atom VUV LIF signal recorded at 50 K as a function of delay time between lasers is displayed in Figure 1 in the presence and absence of NO.

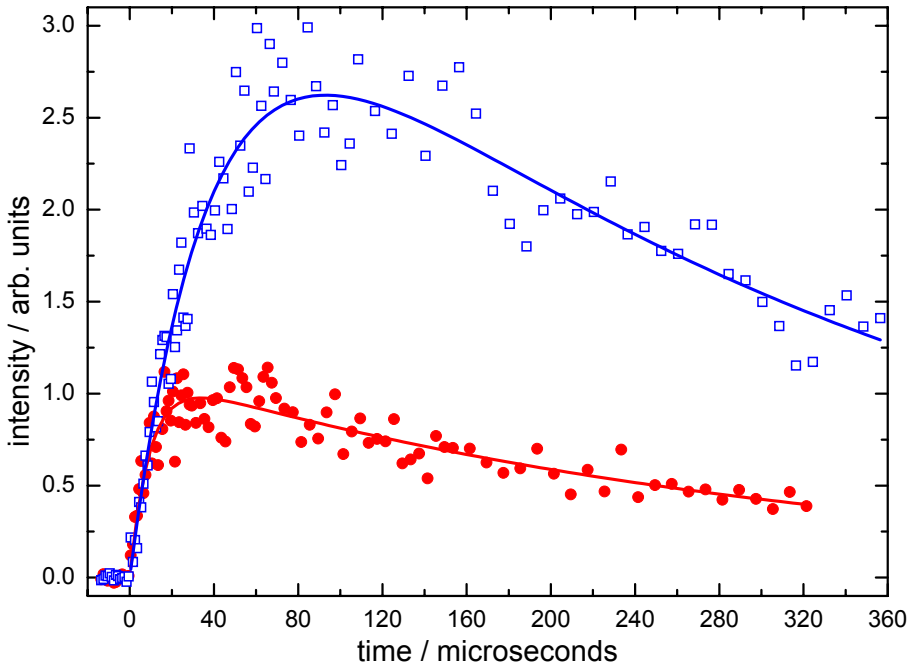

Figure 1 H-atom formation curves recorded at 50 K for the C(^{1}D) + NO reaction using the H_2 chemical tracer method. (Open blue squares) without NO, [H_2] = 1.2 × 10^{14} cm^{-3}; (solid red circles) [NO] = 8.9 × 10^{14} cm^{-3}, [H_2] = 1.2 × 10^{14} cm^{-3}. Solid blue and red lines represent biexponential fits to the individual datapoints using expression (1).

It is clear from Figure 1 that the amplitude of the H atom fluorescence signal is smaller when NO is present in the flow. Indeed, the signal amplitude decreased at higher [NO], with a similar effect being observed for the C(^{1}D) + O_2 reaction. In addition, when NO or O_2 are added the peak of the H-atom formation curve is shifted to shorter times. As higher coreagent NO or O_2 concentrations promote faster removal of C(^{1}D) atoms (C(^{1}D) is removed by other species in the flow at a constant rate), fewer C(^{1}D) atoms were available to produce H-atoms through the C(^{1}D) + H_2/CH_4 reactions in such experiments. At least 18 different curves were recorded for each temperature with a minimum of 6 different O_2 or NO coreagent concentrations. The

pseudo-first-order rate constants were plotted as a function of the coreagent concentration to obtain the second-order rate constant for a given reaction at a given temperature, through a weighted linear least-squares fit to the data. Several examples of these fits are shown in Figure 2 for both the $C(^1D) + NO$ (upper panel) and $C(^1D) + O_2$ (lower panel) reactions.

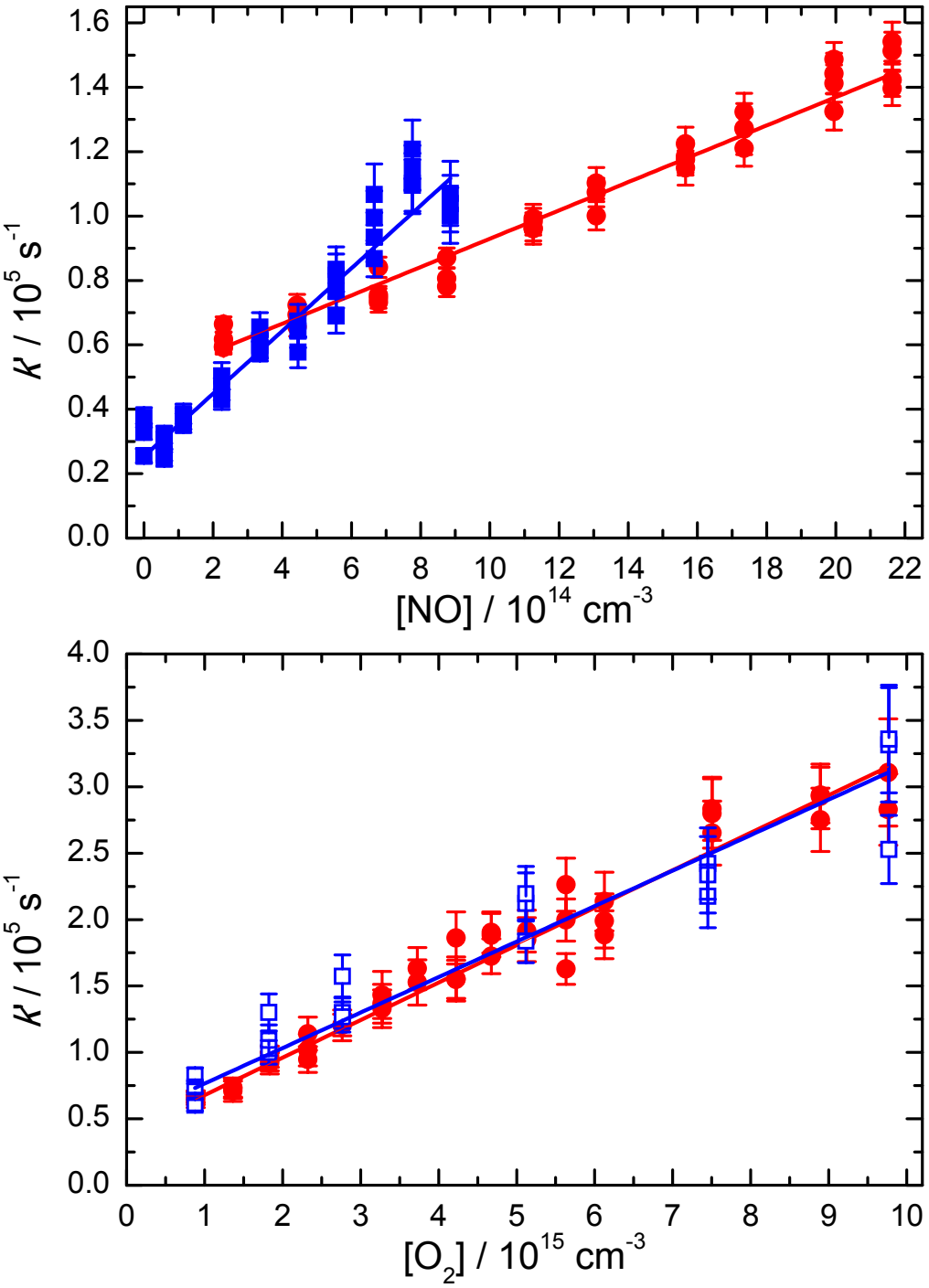

Figure 2 Pseudo-first-order rate constants as a function of coreagent concentration. Top panel: the C(^{1}D) + NO reaction; (solid blue squares) 50 K; (solid red circles) 296 K. Bottom panel:

the $C(^1D) + O_2$ reaction at 127 K; (solid red circles) data recorded with H_2 as the chemical tracer; (open blue squares) data recorded with CH_4 as the chemical tracer. The error bars represent the statistical uncertainty (a single standard deviation) derived from fits to kinetic profiles such as those shown in Figure 1. The second-order rate constants were derived from weighted linear least squares fits to the data (blue and red solid lines).

The derived second-order rate constants are listed in Table 2 and displayed as a function of temperature in Figure 3. The quoted uncertainties represent the combined statistical and systematic errors. The statistical errors were derived from weighted fits such as those shown in Figure 2. The systematic errors are estimated at the level of 20 % of the nominal rate constant value for the present investigation given the potential for secondary reactions to interfere with the primary processes.

Table 2 Measured rate constants for the $C(^1D) + NO$ and $C(^1D) + O_2$ reactions.

T / K	N[b]	$[H_2]$ / 10^{14} cm^{-3}	[NO] / 10^{14} cm^{-3}	$k_{C(1D)+NO}$ / 10^{-11} cm^3 s^{-1}	N	$[H_2]/[CH_4]$ / 10^{14} cm^{-3}	$[O_2]$ / 10^{15} cm^{-3}	$k_{C(1D)+O2}$ /10^{-11} cm^3 s^{-1}
296	37	1.4	2.3-21.6	(4.4 ± 0.9)[c]	39	1.4[d]	1.2-10.1	(2.8 ± 0.6)
					35	0.7[e]	1.2-10.2	(3.1 ± 0.7)
127±2[a]	11	0.7	0-13.1	(4.8 ± 1.1)	41	1.7[d]	0.9-9.8	(2.8 ± 0.6)
	35	1.7	0-16.3	(5.1 ± 1.0)				
	12	3.5	3.3-16.4	(5.5 ± 1.4)	18	0.5[e]	0.9-9.8	(2.7 ± 0.6)
75±2	37	0.8	0-8.0	(6.7 ± 1.4)	36	0.9[d]	0.4-7.2	(2.7 ± 0.5)
50±1	36	1.2	0-8.9	(9.7 ± 2.0)	41	1.2[d]	0.6-9.7	(3.4 ± 0.7)

[a]Uncertainties on the calculated temperatures represent the statistical (1σ) errors obtained from Pitot tube measurements of the impact pressure. [b]Number of individual measurements;

[c]Uncertainties on the measured rate constants represent the combined statistical and systematic errors as explained in the text. [d]Rate constants determined with H_2 as the chemical tracer. [e]Rate constants determined with CH_4 as the chemical tracer.

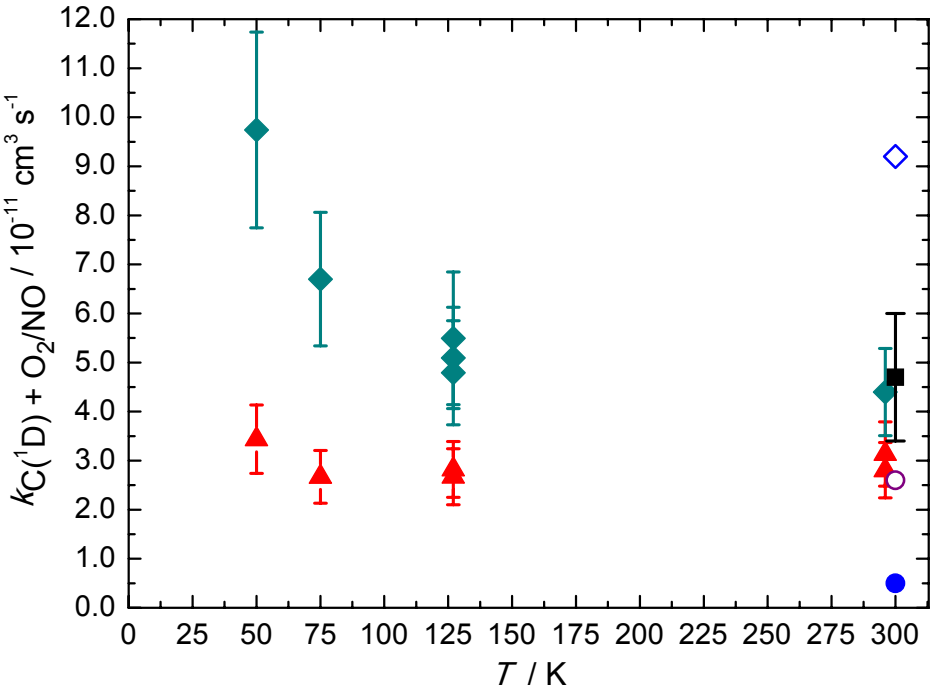

Figure 3 Rate constants for C(^{1}D) reactions as a function of temperature. C(^{1}D) + NO: (solid green diamonds) this work; (solid black square) Husain and Kirsch [32]; (open blue diamond) Braun et al. [35]. C(^{1}D) + O_2: (solid red triangles) this work; (open purple circle) Husain and Kirsch [32]; (solid blue circle) Braun et al [35].

The measured rate constants for the C(^{1}D) + O_2 and C(^{1}D) + NO reactions of $(2.8 \pm 0.3) \times 10^{-11}$ cm^3 s^{-1} and $(4.4 \pm 0.5) \times 10^{-11}$ cm^3 s^{-1} respectively, are seen to be in excellent agreement with the previous study of these processes by Husain and Kirsch at 300 K [32], although these authors state that their rate constant value for the C(^{1}D) + O_2 reaction should be taken with caution given the extent of O_2 photolysis during the experiments. The agreement with the earlier

room temperature results of Braun et al. [35] for both reactions is quite poor. While the $C(^1D)$ + O_2 reaction displays only small variations as a function of temperature in the 50 - 296 K range, the $C(^1D)$ + NO reaction increases rapidly below 100 K, with the rate constant reaching a value of $(9.7 \pm 1.1) \times 10^{-11}$ cm^3 s^{-1} at 50 K; a factor of two increase with respect to the measured value at 296 K.

As the kinetics of the $C(^1D)$ + NO and $C(^1D)$ + O_2 reactions were only followed indirectly in the present experiments, it was necessary to examine the potential effects of secondary reactions on the measured rate constants. Moreover, as $C(^3P)$ atoms are also generated in the reactor as a byproduct of CBr_4 photolysis at 266 nm, it was important to evaluate the influence of the $C(^3P)$ + NO and $C(^3P)$ + O_2 reaction products on the chemistry. In particular, any secondary H-atom sources could interfere with our rate constant measurements of the primary reactions. It is also possible that some $C(^3P)$ atoms might be produced through electronic quenching of $C(^1D)$ by O_2 or NO, although no experimental or theoretical evidence exists for these non-reactive processes.

In the case of the $C(^1D)/C(^3P)$ + O_2 system, previous work [36] indicates that $O(^1D)$ is likely to be a major product for at least one of these processes and should therefore lead to H-atom production through the $O(^1D)$ + $H_2 \rightarrow$ OH + H reaction. To check for the possible influence of secondary H-atom production in our studies of the $C(^1D)$ + O_2 reaction, we employed CH_4 as the H-atom source in additional experiments performed at 127 K and at 296 K. While the H-atom yield of the $C(^1D)$ + CH_4 reaction is close to unity over a wide temperature range [26], the corresponding $O(^1D)$ + CH_4 reaction leads to only a 20 % yield of secondary H-atom products (with CH_3O/CH_2OH as the coproduct) [37], in stark contrast to the $O(^1D)$ + H_2 reaction with a 100 % H-atom yield [38]. Consequently, if H-atom formation through secondary reactions of $O(^1D)$ atoms is important, we would expect to observe a noticeable difference between those experiments employing CH_4 and those experiments employing H_2 as the H-atom

source. The lower panel of Figure 2 shows the results of two such experiments conducted at 127 K, with both methods essentially leading to the same value for the second-order rate constant.

In the case of the $C(^1D)/C(^3P)$ + NO system, we also had to account for the reaction of ground state $C(^3P)$ atoms with NO which is known to lead to several different bimolecular products. Previous work by Bergeat et al. [27] has established that this reaction leads to 60 % production of atomic nitrogen ($N(^4S) + N(^2D)$) with the remaining 40 % leading to $O(^3P)$ formation at room temperature. Of these channels, the formation of $N(^2D)$ will lead to secondary H-atom formation through the $N(^2D) + H_2 \rightarrow NH + H$ reaction. Moreover, the $C(^1D)$ + NO reaction itself could lead to $O(^1D)$ formation (in addition to the $N(^2D)$ channel), as $CN(X^2\Sigma^+) + O(^1D)$ products are also adiabatically and energetically accessible for these reagents. Consequently, the reactions of $O(^1D)$ and $N(^2D)$ with H_2 could both lead to secondary H-atom formation. To test for the possible influence of these reactions, we ran additional test experiments at 127 K to determine the rate constant for the $C(^1D)$ + NO reaction. In these experiments, H-atom formation profiles were recorded for a range of NO concentrations using three different fixed H_2 concentrations ($[H_2]$ = 0.7, 1.7 and 3.5 × 10^{14} cm^{-3}). The resulting pseudo-first-order rates were plotted against the corresponding NO concentration as shown in Figure S1. As expected, the y-axis intercept value increases with increasing H_2, due to the increased rate of H-atom formation. Although the derived second-order rate constant is seen to increase slightly with H_2 as shown by the slopes of the three datasets in Figure S1, the values are essentially identical when the experimental error bars are considered, as shown in Figure 3.

As a secondary check of the overall chemistry, numerical simulations of the reactions potentially involved in the C + O_2 and C + NO systems were also performed using the differential integrator FACSIMILE. The reactions used in the simulations are listed in Tables S1 and S2 alongside their corresponding references when available [18, 26, 27, 31, 37-47]. The

branching ratios and/or temperature dependences for several of these processes are unknown, so it was necessary to estimate these quantities for a meaningful comparison with the experimental results. The aim of the simulations was to generate H-atom formation profiles over a similar range of reagent concentrations to those used in the experiments. These H-atom profiles were then fitted using expression (1), yielding a range of values for k'_F at a given temperature so that simulated second-order rate constants $k_{SIM}(T)$ for the $C(^1D) + O_2$ and $C(^1D)$ + NO reactions could be extracted from the slopes of simulated second-order plots. A comparison between the simulated and experimental H-atom profiles is shown in Figure S2. The simulated second-order rate constants were then compared with the assumed input value used in the simulation, to check for any significant deviations brought about by secondary chemistry. Given the large uncertainties in the branching ratios and rate constants for several important reactions used in the simulations, we estimate an uncertainty of at least 20 % on the resulting simulated rate constants. This value was determined through a sensitivity analysis by varying the rate constants of most important secondary processes. For the $C + O_2$ system, simulations were performed with both H_2 and CH_4 as the primary H-atom sources in a similar manner to the experiments. The excess reagent concentrations were obtained directly from their partial pressures and the initial $C(^1D)$ and $C(^3P)$ concentrations were estimated from the gas-phase concentration of CBr_4 and its absorption cross-section along with the photolysis laser fluence. For the $C(^1D) + O_2$ reaction, the simulated second-order rate constants at 50, 75 and 127 K are within 4 % of the input value when using H_2 as H-atom source. At room temperature, the simulated rate constant is 21 % lower than the input value, indicating that secondary H-atom formation could lead to an error in the measured rate at this temperature. When the same simulations are performed at 296 K and 127 K using CH_4 as the H-atom source, the deviations are reduced to less than 13 % at 296 K (the value at 127 K is within 4 % of the input value). The larger discrepancy in simulations employing H_2 arises mostly from the reaction of CH

(produced by the $C(^1D) + H_2$ reaction) with O_2, leading to atomic hydrogen as a major product (channels 7a and 7c in Table S1). $O(^1D)$ atoms produced by reaction 3a were also thought to be an important source of H-atoms in the simulations through the $O(^1D) + H_2$ reaction (reaction 6). However, when the branching ratio of this channel is set to zero, the discrepancy between the input and output rate constants for reaction 1 increases slightly at all temperatures, clearly indicating the influence of non-linear effects in this complex system of coupled reactions. When CH_4 is used as the H-atom source, the only secondary process leading to H-atom production is the $O(^1D) + CH_4$ reaction (reaction 11b) with a much smaller yield than the $O(^1D) + H_2$ one [37]. Nevertheless, as our room temperature measurements of the $C(^1D) + O_2$ reaction with H_2 and CH_4 result in very similar second-order rate constants, this might indicate that the real branching ratios for the H-atom production channels of the $CH + O_2$ reaction (7a and 7c) are smaller than the ones used in the simulations.

For the $C(^1D) + NO$ reaction, where only H_2 was used as the H-atom source, the discrepancy between the simulated second-order rate constants and the input value increases as the temperature decreases, from 5 % at 296 K to 25 % at 50 K. The reactions that are responsible for most of this effect are those leading to $O(^1D)$ formation, as these atoms react rapidly with H_2 to form atomic hydrogen (reaction 6). Indeed, if reaction 6 is switched off in the simulations, the discrepancy between the input and output second order rate constants decreases to a maximum of 10 % at 50 K. In particular, the reaction of $N(^2D)$ atoms with NO (reaction 17a) is the major source of $O(^1D)$ atoms in these simulations, with $N(^2D)$ atoms being mostly produced by the reaction of ground state carbon atoms with NO (reaction 13b). As earlier measurements by Bergeat et al. [27] only yielded the sum of N-atom production channels (reactions 13a + 13b) for this reaction, we set the rate constants for each of these channels to 30 % of the total reaction rate. Consequently, it is possible that $N(^2D)$ production is

overestimated in these simulations. Moreover, the branching ratios for the individual channels of the N(^{2}D) + NO reaction have never been measured [45].

We also tested the effect of varying the H_2 concentration for the C(^{1}D) + NO simulations at 127 K, to validate the measurements performed at three different H_2 concentrations. With [H_2] = 0.7 and 1.7 × 10^{14} cm^{-3}, the simulated second-order rate constants are identical, with a value of 4.6 × 10^{-11} cm^3 s^{-1} (using the input value of 5.1× 10^{-11} cm^3 s^{-1}). With [H_2] = 3.5 × 10^{14} cm^{-3}, the simulated second-order rate constant rises to 5.2 × 10^{-11} cm^3 s^{-1}. The main experiments at 127 K were all performed using [H_2] = 1.7 × 10^{14} cm^{-3}.

It is interesting to compare the present results for the C(^{1}D) + NO and C(^{1}D) + O_2 reactions with previous work on the equivalent ground state carbon atom reactions. Chastaing et al. [3] and Geppert et al. [31] investigated the kinetics of the C(^{3}P) + O_2 and C(^{3}P) + NO reactions over an extended temperature range (15-295 K). They found that the C(^{3}P) + O_2 reaction becomes faster as the temperature falls with rate constants ranging from (4.09 ± 0.16) × 10^{-11} cm^3 s^{-1} at 295 K to (11.2 ± 0.7) × 10^{-11} cm^3 s^{-1} at 15 K, in contrast with our measured rate constants for the C(^{1}D) + O_2 reaction which do not display a marked temperature dependence. Chastaing et al. [2] hypothesized that the increase in reaction rate as the temperature decreases could originate from the changing population distribution over spin-orbit levels of C(^{3}P) which will be at thermal equilibrium in Laval nozzle type flows due to collisions with the carrier gas. If reaction occurs adiabatically, only from specific spin-orbit states, this could lead to large changes in the overall reaction rate as the temperature is varied. In the case of the C(^{1}D) + O_2 reaction, the fine structure states of the C($^1D_2$) atom are degenerate so that the population distribution is unaffected by temperature. In this instance, a comparable effect will not occur for the excited state carbon atom reaction with O_2.

For the C(^{3}P) + NO reaction, Chastaing et al. [3] showed that the rate constants increased slightly with decreasing temperature from (1.2 ± 0.09) × 10^{-10} cm^3 s^{-1} at 295 K to (2.28 ± 0.17)

$\times 10^{-10}$ cm^3 s^{-1} at 15 K in a similar manner to our results for the corresponding C(^{1}D) atom reaction which displays a twofold increase in reactivity over the 50 K - 296 K range (although the C(^{3}P) atom reaction is 3 to 4 times faster than the C(^{1}D) atom one). In the case of the C(^{3}P) + NO reaction, the situation is particularly complex with C(^3P_J) and NO($^2\Pi_\Omega$) reagents correlating with 36 different states, 18 of which correlate with exothermic products O(^{3}P) and CN($X^2\Sigma^+$) [48]. Consequently, the changing spin-orbit populations of both C(^3P_J) and NO($^2\Pi_\Omega$) could result in a wide range of temperature dependences, as certain adiabatic product channels become more or less favored as the temperature changes. In the case of the C($^1D_2$) + NO($^2\Pi_\Omega$) reaction, only the population distribution of the spin-orbit levels of NO changes as a function of temperature. As a result, we might expect to observe a negative temperature dependence for this process if reaction between C($^1D_2$) and ground electronic state NO($^2\Pi_{1/2}$) is one of the preferred pathways.

Interestingly, the reactions of C(^{1}D) with the radical species O_2 and NO display rate constants that are smaller than those of the reactions of C(^{1}D) atoms with closed shell molecules in general [32]. This is likely to be related to the large number of electronic states correlating adiabatically with both sets of reagents, leading to small electronic degeneracy factors (that is the fraction of the thermal population on reactant electronic states that lead to product formation) and a correspondingly lower reactivity.

4 Conclusions

We have measured rate constants for the reactions of excited state carbon atoms, C(^{1}D), with oxygen bearing molecules O_2 and NO over the 50 - 296 K temperature range using a supersonic flow reactor. Pulsed laser photolysis was employed to generate C(^{1}D) atoms and a chemical tracer method, based on the addition of either H_2 or CH_4 to the flow, was used to follow the progress of the reaction. H-atoms produced by the tracer reaction were detected by vacuum

ultraviolet laser induced fluorescence. The rate constants for the $C(^1D) + O_2$ reaction vary only slightly over the experimental temperature range. In contrast, the rate constants for the $C(^1D)$ + NO reaction increase as the temperature falls. As these reactions could not be followed directly, various test measurements were performed to validate the measured rate constants. In addition, numerical simulations were performed to evaluate the impact of secondary reactions on the rate constant measurements. Taken together, the test measurements and simulations indicate that secondary reactions have only a minor influence on the derived rate constant values.

Acknowledgements

K.M.H. and D.N.R acknowledge support from the French program "Physique et Chimie du Milieu Interstellaire" (PCMI) of the CNRS/INSU with the INC/INP co-funded by the CEA and CNES.

References

[1] D.C. Clary, N. Haider, D. Husain, M. Kabir, ApJ. 422 (1994) 416.
[2] D. Chastaing, P.L. James, I.R. Sims, I.W.M. Smith, Phys. Chem. Chem. Phys. 1 (1999) 2247.
[3] D. Chastaing, S.D. Le Picard, I.R. Sims, J. Chem. Phys. 112 (2000) 8466.
[4] D. Chastaing, S.D. Le Picard, I.R. Sims, I.W.M. Smith, W.D. Geppert, C. Naulin, M. Costes, Chem. Phys. Lett. 331 (2000) 170.
[5] K.M. Hickson, J.-C. Loison, D. Nuñez-Reyes, R. Méreau, J. Phys. Chem. Lett. 7 (2016) 3641.
[6] K.M. Hickson, J.-C. Loison, J. Bourgalais, M. Capron, S.D. Le Picard, F. Goulay, V. Wakelam, ApJ. 812 (2015) 107.
[7] R.J. Shannon, C. Cossou, J.-C. Loison, P. Caubet, N. Balucani, P.W. Seakins, V. Wakelam, K.M. Hickson, RSC Adv. 4 (2014) 26342.
[8] J. Bourgalais, M. Capron, R.K.A. Kailasanathan, D.L. Osborn, K.M. Hickson, J.-C. Loison, V. Wakelam, F. Goulay, S.D. Le Picard, ApJ. 812 (2015) 106.
[9] D.C. Clary, E. Buonomo, I.R. Sims, I.W.M. Smith, W.D. Geppert, C. Naulin, M. Costes, L. Cartechini, P. Casavecchia, J. Phys. Chem. A. 106 (2002) 5541.
[10] R.I. Kaiser, A.M. Mebel, Int Rev Phys Chem. 21 (2002) 307.
[11] M. Costes, P. Halvick, K.M. Hickson, N. Daugey, C. Naulin, ApJ. 703 (2009) 1179.
[12] C. Naulin, N. Daugey, K.M. Hickson, M. Costes, J. Phys. Chem. A. 113 (2009) 14447.
[13] F. Leonori, R. Petrucci, E. Segoloni, A. Bergeat, K.M. Hickson, N. Balucani, P. Casavecchia, J. Phys. Chem. A. 112 (2008) 1363.
[14] Z. Shen, H. Ma, C. Zhang, M. Fu, Y. Wu, W. Bian, J. Cao, Nat. Commun. 8 (2017) 14094.
[15] N. Balucani, G. Capozza, E. Segoloni, A. Russo, R. Bobbenkamp, P. Casavecchia, T. Gonzalez-Lezana, E. J. Rackham, L. Bañares, F. J. Aoiz, J. Chem. Phys. 122 (2005) 234309.
[16] N. Balucani, P. Casavecchia, F. J. Aoiz, L. Bañares, J. M. Launay, B. Bussery-Honvault, P. Honvault, Mol. Phys. 108 (2010) 373.
[17] N. Balucani, G. Capozza, L. Cartechini, A. Bergeat, R. Bobbenkamp, P. Casavecchia, F. J. Aoiz, L. Bañares, P. Honvault, B. Bussery-Honvault, J. M. Launay, Phys. Chem. Chem. Phys. 6 (2004) 4957.
[18] K.M. Hickson, J.-C. Loison, H. Guo, Y.V. Suleimanov, J. Phys. Chem. Lett. 6 (2015) 4194.
[19] K.M. Hickson, Y.V. Suleimanov, Phys. Chem. Chem. Phys. 19 (2017) 480.
[20] S.Y. Lin, H. Guo, J. Phys. Chem. A. 108 (2004) 2141.

[21] P. Defazio, B. Bussery-Honvault, P. Honvault, C. Petrongolo, J. Chem. Phys. 135 (2011) 114308.
[22] F. Leonori, D. Skouteris, R. Petrucci, P. Casavecchia, M. Rosi, N. Balucani, J. Chem. Phys. 138 (2013) 024311.
[23] R. I. Kaiser, T. L. Nguyen, A. M. Mebel, Y. T. Lee, J. Chem. Phys. 116 (2002) 1318.
[24] R. I. Kaiser, A. M. Mebel, Y. T. Lee, J. Chem. Phys. 114 (2001) 231.
[25] K.M. Hickson, J.-C. Loison, F. Lique, J. Kłos, J. Phys. Chem. A. 120 (2016) 2504.
[26] D. Nuñez-Reyes, K.M. Hickson, J. Phys. Chem. A. 121 (2017) 3851.
[27] A. Bergeat, T. Calvo, G. Dorthe, J.-C. Loison, Chem. Phys. Lett. 308 (1999) 7.
[28] D. Husain, A.N. Young, J. Chem. Soc., Faraday Trans. 2. 71 (1975) 525.
[29] K.H. Becker, K.J. Brockmann, P. Wiesen, J. Chem. Soc., Faraday Trans. 2. 84 (1988) 455.
[30] G. Dorthe, P. Caubet, T. Vias, B. Barrère, J. Marchais, J. Phys. Chem. 95 (1991) 5109.
[31] W.D. Geppert, D. Reignier, T. Stoecklin, C. Naulin, M. Costes, D. Chastaing, S.D. Le Picard, I.R. Sims, I.W.M. Smith, Phys. Chem. Chem. Phys. 2 (2000) 2873.
[32] D. Husain, L.J. Kirsch, Trans. Faraday Soc. 67 (1971) 3166.
[33] N. Daugey, P. Caubet, B. Retail, M. Costes, A. Bergeat, G. Dorthe, Phys. Chem. Chem. Phys. 7 (2005) 2921.
[34] N. Daugey, P. Caubet, A. Bergeat, M. Costes, K.M. Hickson, Phys. Chem. Chem. Phys. 10 (2008) 729.
[35] W. Braun, A.M. Bass, D.D. Davis, J.D. Simmons, Proc. Roy. Soc. A. 312 (1969) 417.
[36] W. D. Geppert, C. Naulin, M. Costes, Chem. Phys. Lett. 364 (2002) 121.
[37] Q. Meng, K.M. Hickson, K. Shao, J.-C. Loison, D.H. Zhang, Phys. Chem. Chem. Phys. 18 (2016) 29286.
[38] K.M. Hickson, Y.V. Suleimanov, J. Phys. Chem. A. 121 (2017) 1916.
[39] R. Grondin, J.-C. Loison, K.M. Hickson, J. Phys. Chem. A. 120 (2016) 4838.
[40] A. Bergeat, T. Calvo, F. Caralp, J.-H. Fillion, G. Dorthe, J.-C. Loison, Faraday Discuss. 119 (2001) 67.
[41] P. Bocherel, L.B. Herbert, B.R. Rowe, I.R. Sims, I.W.M. Smith, D. Travers, J. Phys. Chem. 100 (1996) 3063.
[42] R.A. Brownsword, A. Canosa, B.R. Rowe, I.R. Sims, I.W.M. Smith, D.W.A. Stewart, A.C. Symonds, D. Travers, J. Chem. Phys. 106 (1997) 7662.
[43] C.-L. Lin, F. Kaufman, J. Chem. Phys. 55 (1971) 3760.
[44] A. Bergeat, T. Calvo, N. Daugey, J.-C. Loison, G. Dorthe, J. Phys. Chem. A. 102 (1998) 8124.
[45] J.T. Herron, J. Phys. Chem. Ref. Data, 28 (1999) 1453.
[46] J. Li, P.J.S.B. Caridade, A.J.C. Varandas, J. Phys. Chem A. 118 (2014) 1277.
[47] R.J. Donovan, D. Husain, Chem. Rev. 70 (1970) 489.
[48] S. Andersson, N. Markovic, G. Nyman, J. Phys. Chem A. 107 (2003) 5439.